QUARTZ CRYSTAL MICROBALANCE ADSORPTION APPARATUS FOR HIGH PRESSURE GAS ADSORPTION MEASUREMENTS IN NANOMATERIALS

A Thesis
Presented to
The Academic Faculty

by

Milad Navaei

In Partial Fulfillment
of the Requirements for the Degree
Master of Science in the
G.W. Woodruff School of Mechanical Engineering

Georgia Institute of Technology
Aug 2011

QUARTZ CRYSTAL MICROBALANCE ADSORPTION APPARATUS FOR HIGH PRESSURE GAS ADSORPTION MEASUREMENTS IN NANOMATERIALS

Approved by:

Dr. Peter Hesketh, Advisor

School of Mechanical Engineering

Georgia Institute of Technology

Dr. Sankar Nair

School of Chemical & bimolecular engineering

Georgia Institute of Technology

Dr. Todd Sulchek

School of Mechanical Engineering

Georgia Institute of Technology

Date Approved: April 6th 2011

To my parents
for their love, endless support and encouragement.

ACKNOWLEDGEMENTS

I would like to express my sincere appreciation to my advisor, Dr. Peter Hesketh for his endless support and guidance during my studies. I am grateful for having him as my advisor for his insight and career advice. I would like to thank the committee members Dr. Sankar Nair and Dr. Todd Sulchek for their suggestions and willingness to help. Measurements

I am also grateful to all my colleagues in Hesketh and Nair research group for their valuable discussions and suggestions. I like to thank Mr. Dun-Yen Kang for providing the nanotubes, and Mr. Casey Timmerman and Matthew Arinez for their assistance in assembling the experimental facility and data acquisition.

I acknowledge ConocoPhillips for supporting this research, and Dr. Ken McCarley research group for providing the Polyimide samples.

TABLE OF CONTENTS

LIST OF TABLES

LIST OF FIGURES

SUMMARY

The primary objective of this study was to develop a sensitive and cost-effective sorption system to analyze adsorption and diffusion of different gases on micro porous materials and nanotubes. A high pressure Quartz Crystal Microbalance (QCM) based adsorption apparatus for single-component gas was developed. A QCM is an acoustic-wave resonator in which the acoustic wave propagates through the crystal. Therefore, it is highly responsive to addition or removal of small amounts of mass adsorbed or deposited on the surface of the crystal. This mass sensitivity makes the QCM an ideal tool for the study of gas adsorption. The QCM-based adsorption apparatus is advantageous over the commercialized none-gravimetric and gravimetric equipment in a way that it is low-cost, highly sensitive and accurate for mass sorption applications, satisfactorily stable in a controlled environment, and can be used for thin films.

The high pressure apparatus was calibrated using Matrimid 5218, whose thermodynamic properties and adsorption parameters are known. The Matrimid was spin-coated onto a 14 mm-diameter QCM, and sorption equilibrium data for were obtained for CO_2 gas at 25, 30, 48, and 52 ºC and partial pressure range between 0 to 4 bar. In order to compare the experimental data with available literature data, the experimental data was fitted into a dual-mode adsorption model. The model results from Henry's law and a Langmuir mechanism. Comparison of the experimental adsorption isotherm of Matrimide for CO_2 gas with literature data showed reasonable agreement between the experimental and literature data.

In this study, the adsorption parameters of aluminosilicate nanotubes are observed. Aluminosilicate nanotubes are ideal materials for chemical sensing, molecule separation, and gas storage; hence, there is a need for adsorption and diffusion data on this material.

The adsorption of CO_2, N_2, and CH_4 gases on aluminosilicate nanotubes samples has been studied in the temperature range of 20° to 120° Celsius and pressure range of 0 to 8 bar. The experimental results yield the CO_2 and N_2 heat of adsorptions of -32.9 and -28.1 kJ/mol respectively.

CHAPTER 1

INTRODUCTION

1.1 Theory of quartz crystal microbalance

Over the past decade, interest has been increasing in the expansion of Quartz Crystal Microbalance (QCM) principals in sensitive devices such as film deposition monitoring, DNA biosensors, and gas phase detection. QCM is an acoustic-wave sensor in which the acoustic wave propagates in the direction perpendicular to the crystal surface. The basic principle behind all acoustic-wave sensors is that adding mass on the surface of the sensor causes the resonant frequency to decrease. The schematic of a 5 MHz quartz crystal is shown in Figure 1.1. As shown in that figure, QCM consists of three components: top side electrode, bottom side electrode, and quartz dielectric. The top and bottom electrodes, whose lateral dimensions are much smaller than their thickness, are assumed to be thin films with infinite extensions. These two electrodes connect the electrical circuit for two main reasons: to obtain resonant frequency measurement and to stimulate motion. The quartz plane, which is bound within the two electrodes, has a piezoelectric nature, which, by applying AC voltage induces an acoustic wave at the frequency of excitation. Quartz is an essential part of the QCM due to its piezoelectric property.

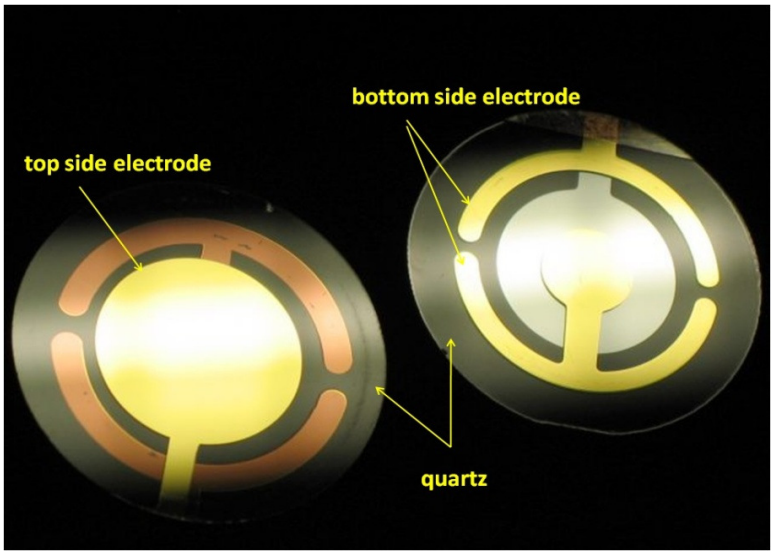

Figure 1.1. Photograph of quartz crystal microbalance

The piezoelectric effect is an electrical depolarization of molecules by subjecting the material to external stress. Application of a small compression force on the material, alters the balance of negative and positive charges of the molecule coincide, causing a depolarization of the molecules. The dipole molecules inside the material cancel each other; therefore, the surfaces of the material become polarized. Surface polarization generates an electric field, resulting in a flow of electric charges in the direction of electric field. After removing force from the material, the polarization disappears, and the material comes back to its initial stage. By decompressing the material, the surface of the material becomes polarized; however, the flow of electric charges is in the opposite direction of the flow of electric charges in the compression force. This phenomenon as shown in Figure 1.2 is called the direct piezoelectric effect in which an electric charge is generated by applying stress on the materials. Figure 1.2 shows when pressure is applied to a material, the dipoles change / the polarization changes, and the electric field changes.

When pressure is removed, the system reverts to its previous state of charge / polarization.

The reverse piezoelectric effect occurs when applied voltage across the piezoelectric material causes strain. [1] This effect is the primary component of QCMs.

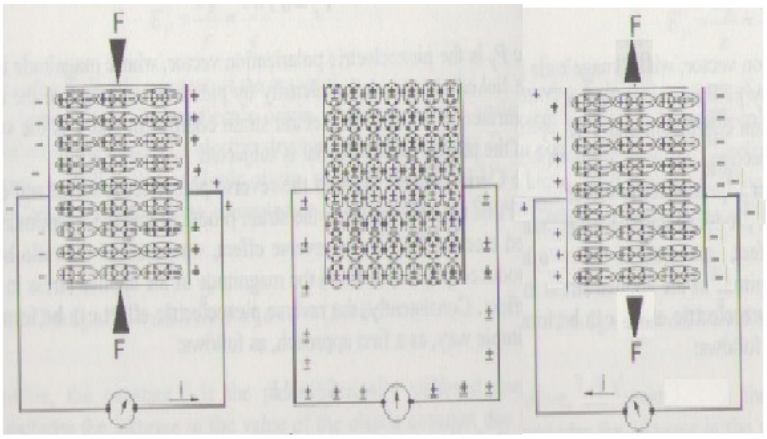

Figure 1.2.Piezoelectric phenomenon *[1]*

The circuit model of QCM is shown in Figure 1.3. The electrical circuit consists of two branches: The motional branch and the static or shunch branch. The motional branch contains L.R.C circuitry that models the motion occurrence and is modified by mass and viscous loading of crystal. The static or shunch branch contains only the capacitance and it is associated with the dielectric materials between the two electrodes.

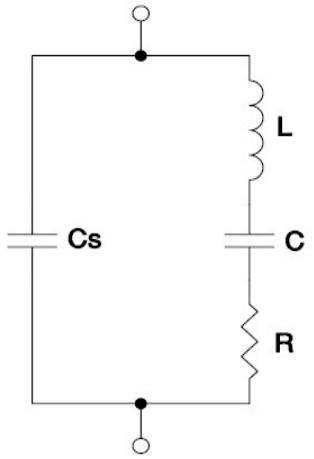

Figure 1.3.The QCM electrical circuit model

The resonant frequency of thick shear mode quartz is a transverse acoustic wave bouncing between the top and bottom electrodes. The resonant frequency of QCM is inversely proportional to the thickness of the crystal as shown in equation 1.1

$$f = n\frac{v_0}{2\times L} \qquad \text{n=1,2,3,..} \tag{1.1}$$

Where f is the resonant frequency, L is the thickness of the quartz plate, V_0 is the speed of sound within the crystal.

One of the advantages of using quartz crystal resonators in sensing applications is associated with a specific crystal cut, at which the temperature coefficient of the crystal frequency is zero. At this point, the frequency change due to the temperature variation is minimized. Figure 1.4 and Figure 1.5 show the frequency change as a function of temperature for 25ºC and 90ºC cut crystals respectively. For the room cut crystal, the effect of temperature in the range of 15-45 ºC is negligible; however, in a higher

temperature environment, the effect of temperature can have a significant influence on attempts to detect small mass changes.

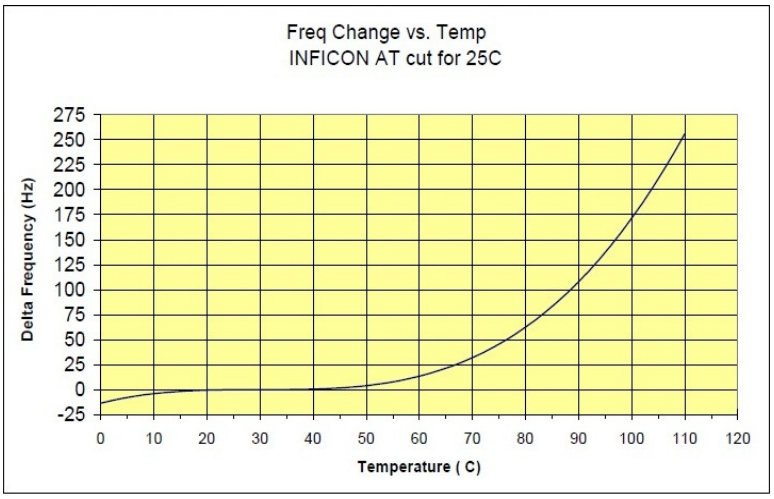

Figure 1.4. Frequency change vs. temperature at º25 C cut

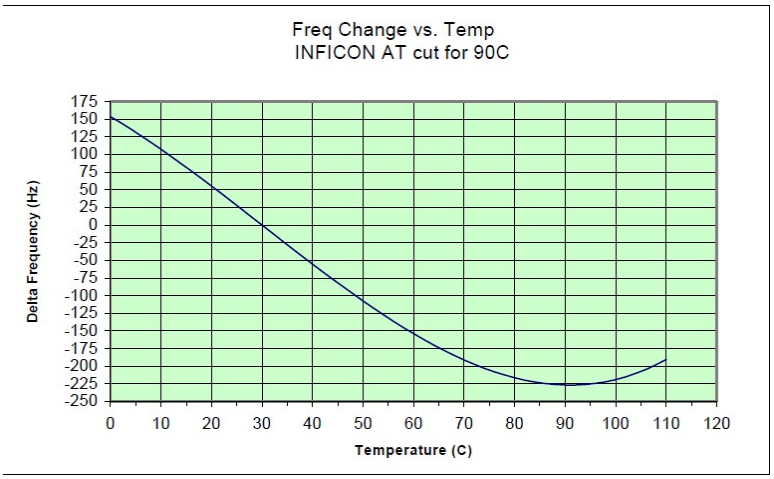

Figure 1.5. Frequency change vs. temperature at º90 C cut

1.1.1 Sauerbrey equation

Sauerbrey was the first to determine the ability of QCM to detect small mass changes on the surface of a crystal. He developed an equation that assumes the mass deposited on the surface of the crystal is functionally equivalent to additional quartz. The mass change on the surface of the resonator due to the resonant frequency change in the gas phase median is given by the Sauerbrey equation. [1]

$$\Delta m = \frac{(f_q - f)\sqrt{\rho_q \times \mu_q}}{2n \times f^2} \qquad (1.2)$$

Where f_q is the resonant frequency at reference state in Hz, f is the resonant frequency of loaded crystal in Hz, ρ_q is the density of quartz (2.648 g.cm^{-3}), and μ_q is the effective piezoelectrically stiffened shear modulus of quartz (2.947×10^{11} g.cm^{-3}). An important assumption that facilitates the Sauerbrey equation is that the additional mass or film deposited on the crystal has the same acoustic-elastic properties as quartz. This assumption is valid only if the total frequency change due to the deposition of nonporous materials or gas molecules on the surface of the resonator is less than 1% of the resonant frequency.

1.1.2 Factors affecting the frequency of QCM

The frequency change of a QCM is not only due to the mass adsorbed or deposited on the surface, but also to the sum of the terms of the form:

$$\Delta f = \Delta f_m + \Delta f_T + \Delta f_P + \Delta f_v + \Delta f_R ,$$

where the terms on the right side of the equation correspond to the shift in frequency due to the change in mass, temperature, hydrostatic pressure, viscosity, and roughness loading, respectively.[2] The effect of temperature on frequency change is given by equation 1.3

$$\Delta f_T = f_0 \beta(T) \tag{1.3}$$

where *B(T)* is negligible in the temperature range between 14 and 45 ºC for room cut QCMs and 90 ºC for 90 ºC cut QCMs. Also, the frequency change due to the hydrostatic pressure is given by equation 1.4.

$$\Delta f_P = f_0 \alpha P \tag{1.4}$$

where P is the hydrostatic pressure and α is the pressure constant. The pressure constant reported by Stockbridge is 1.045×10^{-5} MPa^{-1} at 25ºC.

The effect of viscosity loading on QCM is discussed by Kanazawa using a physics model in the fluid[3].

$$\Delta f_\nu = -f_0^{\frac{3}{2}} \sqrt{\frac{\rho_L n_L}{\pi \rho \mu_L}} \tag{1.5}$$

Where ρ_L is the density of the liquid, n_L is the viscosity of the liquid, ρ is the density of quartz. The frequency change due to the effect of viscosity loading is significant; however, there are some variations in the value of the viscosity coefficient reported for liquid and gas surrounding.

In the end, effect of surface roughness loading is driven by equation 1.6 [4]

$$\Delta f_R = -H \times \rho_L \tag{1.6}$$

H is a constant which depends on the surface roughness and fundamental frequency of the QCM.

In order to eliminate the effects of frequency change due to these terms, an identical reference QCM was placed in the experimental cell next to the coated QCM. After each experiment, the corrections were applied to the frequency of the coated QCM by subtracting it from the frequency of the reference QCM. Using this technique, the frequency change due to the hydrostatic pressure, viscosity loading was eradicated. The effect of roughness loading is assumed to be negligible, since the crystals used in the experiment have both sides polished, hence, the roughness is minimum.

Furthermore, the damping voltage of a QCM is another important factor which needs to be studied. To ensure that the frequency error due to the damping is small for each measurement, Equation 1.7 was used to convert the damping voltage of a QCM to a frequency error.

$$\Delta f = -\frac{\arctan\left(2\pi f_o C_{crystal} R_{crystal}\right)}{2} \frac{f_o}{Q} \tag{1.7}$$

where f_0 is the fundamental frequency (f_0 ~5MHz) , Q is the quality factor, $C_{crystal}$ is the capacitance of the crystal ($C_{crystal}$ =6-7(pF), and $R_{crystal}$ is the resistance of the crystal. The quality factor is the sharpness of the resonant frequency peak and short term stability of an oscillation. The quality factor is defined as the ratio between the mechanical energy and the energy dissipated per cycle due to the QCM oscillation. The quality factor is expressed by equation 1.8

$$\mathrm{Q} = 2\pi \frac{\text{Mechanical energy}}{\text{Energy dissipated per cycle}} \tag{1.8}$$

The quality factor of typical quartz crystal oscillator is around 10^5. The resistance of the crystal was calculated using equation 1.9 as shown below.

$$R_{crystal} = \frac{100}{V_{DC}} - 20 \tag{1.9}$$

Using these parameters in equation 1.7, the frequency error for the experiment is measured to be less than 1 Hz while damping voltage ranges between 3-3.6 V.

1.2 Use of QCM for gas adsorption measurement in thin films.

One of the areas where the use of piezoelectric materials has been expanding recently is the use of QCM for chemical sensing in the gas phase. QCM is a suitable resonator for gas sensing application due to its mass sensitivity, its operational simplicity, and the ease of real time monitoring that QCMs provide. The high sensitivity QCM makes it a suitable device for studying the adsorption of different gases into thin films of nanoporous materials and nanotubes. The use of QCM as a chemical sensor has its origin in the works of Sauerbrey, who developed a gravimetric method in the gas phase. Later on, Tsionsky[5] studied gas adsorption on the surface of QCM in constant pressure. In his work, the pressure inside the cell was maintained constant at all times and only the partial pressure of substance gas and inert gas varied (Sorption gas method). The down side of this method is that the resonant frequency change of QCM is not only due to the amount of substance gas adsorbed on the surface, but also to the amount of inert gas that may be absorbed. Another process mostly used for gas adsorption is the pressure variation method, in which the crystal is placed under vacuum, and the substance gas is slowly introduced into the cell to reach each new equilibrium condition. The advantages of using this method are: the total resonant frequency change is due to the gas adsorbed on the

surface, and no gas mixing and incubating step is required before introducing the gas into the chamber.

1.3 Gas adsorption in single-walled aluminosilicate nanotubes

Nanoporous materials, such as metal-organic framework and single-walled metal oxide nanotubes, have piqued researchers' interest due to their potential applications in molecular separation, chemical sensing, gas storage, catalysis, and other applications which require tailored pore properties.[6-9] One of the advantages of these materials is their potential for gas molecule separation and storage, especially Imogolite, which is a natural product of aluminosilicate nanotubes. These nanotubes have drawn significant interest in recent years due to their porosity, their hollow cylindrical shape, and their uniform structural composition. Aluminosilicate nanotubes consist of a hydroxide layer (OH) on the outer surface, and silanol groups on the inner surface; they have an inner diameter of 1 nm and outer diameter of 2.3 nm as shown in Figure 1.6.

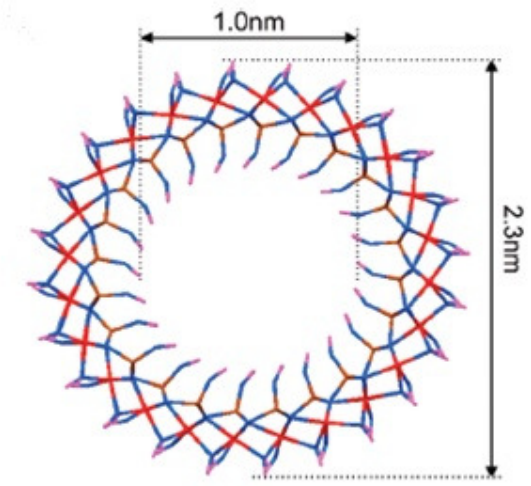

Figure 1.6.Cross-Section view of single-walled aluminosilicate nanotubes

The aluminosilicate nanotubes' synthesis and purification are explained in Dun-Yen Keng's work [10]. In Keng's work, tetraethyl orthosilicate (TEOS) was mixed with aluminum-tri-sec-butoxide. The mixture was added to 10m Mperchloric acid solution with a molar ratio Si:Al:$HClO_4$ = 1.1:2:1. The solution was then diluted with DT water and heated at 95 ºC for 4 days. Next, the solution was brought to room temperature, and 30 wt% ammonia solution was added. The gel was centrifuged at 7000 rpm for 15 minutes. The supernatant was disposed, and a few drops of 10 N hydrochloric acid were added to the gel. The resulting viscous solution was purified by dialysis against DI water for 3 days using a 15 000 Dalton membrane.

1.4 Concluding summary and problem formulation

Considering the above discussion, developing a QCM based high pressure setup with a reference QCM integrated in it is vital to eliminate the factors described in section 1.1.2 and also to study the gas adsorption in thin film of materials. The QCM setup developed in this work is to study gas adsorption into thin films of advance nanomaterials. The experimental data was fit into different model to extract thermodynamic properties of these materials. The QCM-based adsorption apparatus describes in Chapter 2 is advantageous over commercial equipment: it is low-cost, highly sensitive and accurate for mass sorption applications, satisfactorily stable in a controlled environment, and can be used for thin films.

In chapter 3, the experimental setup is calibrated using Matrimid 5215. The CO_2 gas adsorption isotherms of Matrimide is measured using the experimental setup described. The experimental data is compared to the literature data available for these

materials. The comparison between the experimental data and literature data shows good agreement.

In chapter 4, the experimental setup was used to study different gas adsorption in Aluminosilicate nanotubes casted on a QCM. Using two different methods, thermodynamic properties of nanotubes were calculated and reported. These finding is a need for studying gas adsorption and diffusion on this material. Furthermore, these materials could be used in gas purification applications in gas pipelines.

CHAPTER 2

EXPERIMENTAL APPARATUS AND TECHNIQUE

2.1 Design considerations:

The present experimental setup was designed to measure the adsorption of single component gas in thin films deposited on the surface of a QCM. To achieve this measurement, it is necessary to have a method of maintaining the coated QCM and the reference QCM intact inside the isothermal chamber, and to also have a technique to measure the frequency and damping of the crystals continuously. Simultaneously, the experimental setup should be able to stand pressures up to 10 bar and temperatures up to 250 ºC.

2.1.1 High pressure cell

For the experiment, a high pressure cell with an inner diameter of 3 inches, an outer diameter of 4.5 inches, and a height of 2 inches was designed. The total volume of the cell was calculated to be 175 ml. The cell's overall design and cross sectional view are presented in Figure 2.1 and Figure 2.2. One of the constraints in designing the cell was that the total volume of the cell needed to be as small as possible in order to eliminate temperature variation inside the cell.

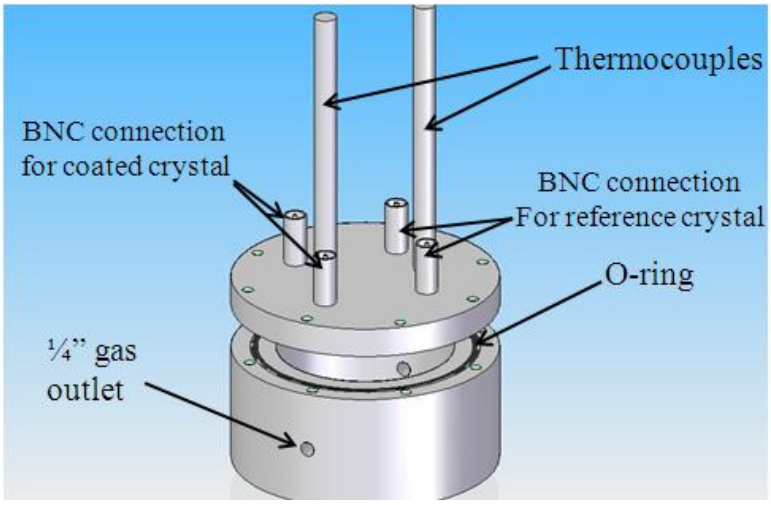

Figure 2.1. High pressure cell overall view

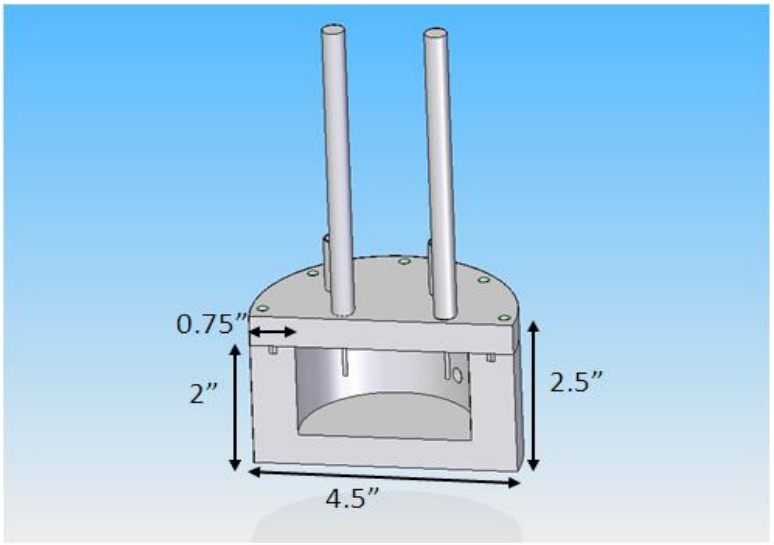

Figure 2.2. Sectional view of the chamber

The two crystals inside the cell were mounted between the electrical connection rings of the crystal holder as shown in Figure 2.3. The electrical connections to the sides of the crystals were made with bent ring-shaped copper wire, and the wires were connected to the back side of a ceramic piece through thresholds. The thresholds were made on the crystal using water jet. The wires were connected to the four BNCs connections screwed onto the cap of the cell. A photograph of the crystal holder with crystals installed is shown in Figure 2.3

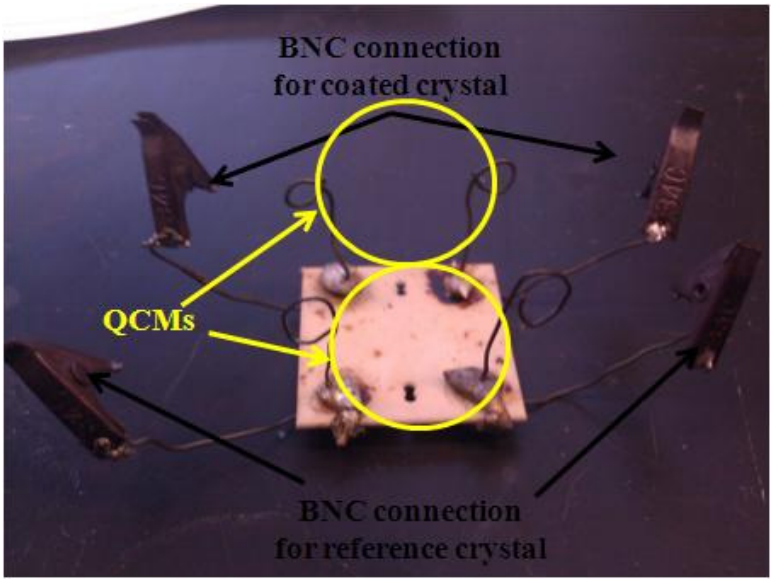

Figure 2.3. Photograph of QCM holder

2.1.2 Temperature monitoring

Two K type thermocouples manufactured by Omega were screwed onto the cap of the cell in two different locations in order to monitor temperature gradients inside the cell. The tips of the thermocouples are half inside the cell as shown in Figure 2.1. The two thermocouples are connected to a cold junction compensator (OMEGA-CJ) through

metal shield wire. The voltage of the cold junction compensator was measured using two multimeters (Agilent 5313X Series), and the voltages were converted to temperatures. The main reason for using two voltmeters was to reduce the Lab View© program's cycle time and consequently improve the accuracy of the readings. Seven-digit voltmeters were used in the setup to ensure temperature accuracy of 0.1 ºC.

2.1.3 Gases

This experimental setup design is capable of running CO_2, N_2, and CH_4 gases; however, the design could easily be modified for water vapor and volatile organic compound (VOCs) experiments. The current setup is connected to these three gases; therefore, no further modification for alternate gas experiments is necessary. The gases used in all the experiments were ultra high purity gases supplied by Airgas (GA). Figure 2.4 shows the connection of the gas cylinders to the setup.

Figure 2.4. Gas cylinders connection to the QCM setup.

A special protocol was made for running the CH_4 experiment due to its explosive nature. The CH_4 gas must be diluted with N_2 gas in a ratio of 1:4 before venting the gas through the vacuum pump, because just a spark in the vacuum pump is capable of igniting the methane. The CH_4 gas ventilation process was as follows: First, the high pressure cell was vented to 15 psi, and then the venting valve was closed. The N_2 gas pressure was set to 60 psi on the regulator and then the N_2 exit valve was opened. After cell pressure reached 60 psi, the N_2 gas exit valve was closed. Next, the atmospheric venting valve was opened, and the cell pressure was allowed to reach 15 psi. These steps were repeated several times to ensure CH_4 gas was diluted enough with N_2. In the end, the high pressure cell was filled with N_2 gas, and the setup was put under vacuum.

2.1.4 QCM resonant frequency measurement

In order to measure the resonant frequency of the crystals, two phase lock oscillators PLO-10, manufactured by Inficon, (NY, USA) were utilized in the setup. A phase lock oscillator was used to drive the crystal oscillation by monitoring the current of the crystal; meanwhile, the frequency of the oscillator is adjusted until there is a zero phase between the crystal's voltage and the current. This zero phase between the crystal's voltage and current is the series resonant point of the crystal. The phase lock had a phase detector which continuously monitored the phase difference between the crystal's current and voltage; hence, the series' resonant frequency automatically adjusted. Figure 2.5 shows the PLO-10 phase locked oscillator.

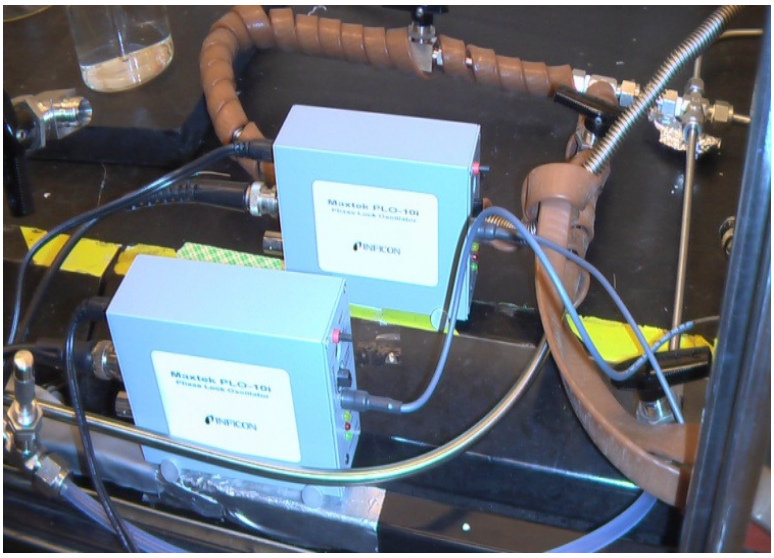

Figure 2.5. Phase locked oscillator utilized in the setup

This phase lock oscillator, which supports 5 MHz crystals, was chosen for its electrode capacitance cancellation, direct time measurement, and auto lock features. Due to the sensitivity of the experiments; the phase lock oscillator is required to have a small frequency error. This phase locked oscillator has a 0.4 Hz frequency error for crystals with quality factor of 10,000, which is suitable for gas adsorption measurement.

2.2 System description

The QCMs employed in this study were commercially available at 5 MHz 25 °C cut; both sides had polished gold electrodes, purchased from Inficon Co (NY, USA). The schematic of the experimental setup is shown in Figure 2.6.

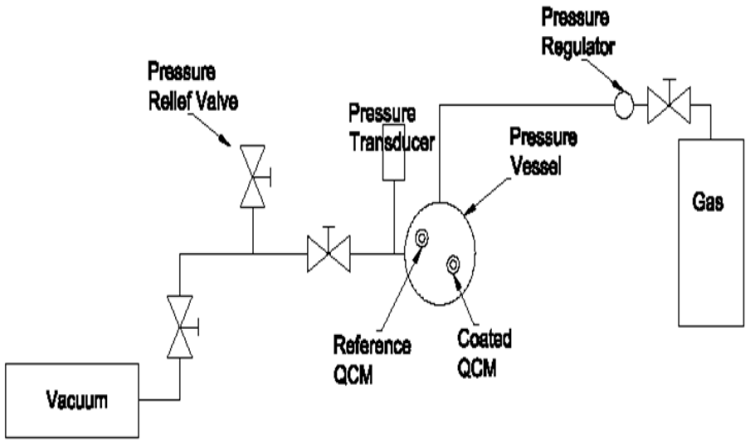

Figure 2.6. Schematic of the experimental setup

Two identical crystals were placed inside the high pressure stainless steel chamber. One crystal was uncoated and acted as a reference, while the other was coated and is to be studied. The chamber was designed to stand pressure and temperature of up to 10 bars and 320 ºC, respectively. The temperature was limited by the maximum operation temperature recommended of the O-ring, which was a MARKEZ® Z1213 PERFLUOROELASTOMER, size 236, manufactured by MARCO RUBBER (NH, USA) and custom designed to seal the chamber at high pressure. The two crystals were connected through four BNCs connections through high-temperature resistant cables

supplied by Omega(USA) to two phase lock oscillators (PLO-10).The output frequencies and damping voltages of both QCMs were measured by a frequency counter (Agilent 5313X Series) and (an/a) Acquisition / Switch unit (*HP 34970A)* for damping voltage. The frequency counter measures 12 digits.s^{-1}, has temperature stability of 2.0E-7/°C, has superior internal time base stability at ultra high oven temperatures, and is capable of measuring frequency to 10 mHz. In order to monitor the absolute pressure inside the cell, a pressure transducer, MKS 10000 Torr (MKS, GA), was fixed to the outlet of the high pressure chamber. This pressure transducer was used to sense the pressure inside the cell continuously and send the signal to the pressure reader PDR200 (MKS, USA).The pressure was controlled by slowly introducing a gas into the cell until each new equilibrium condition was reached. Since the QCMs are extremely temperature sensitive, the high pressure chamber was thermally insulated using glass wool (OHIO VALLY, Ohio), and two semi sphere mantles. A digital temperature controller CG-15001, manufactured by Omega, was used with the mantles to control the temperature with a precision of ± 0.1 °C. A close-up view of the setup is shown in Figure 2.7.

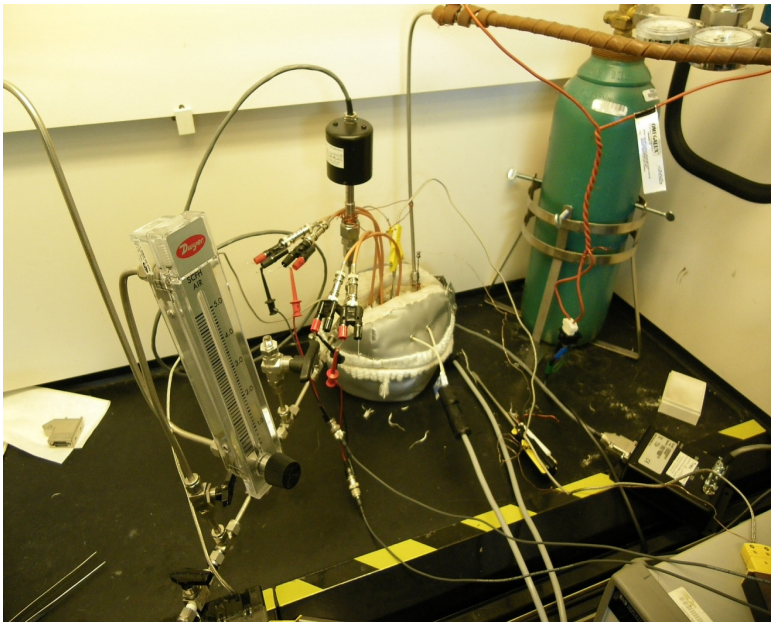

Figure 2.7. Close up view of the high pressure cell and electrical connections

Figure 2.8.Photograph of Experimental setup

The temperatures, frequency, and damping voltages were recorded with Lab View© software on a computer and are presented in Figure 2.9.

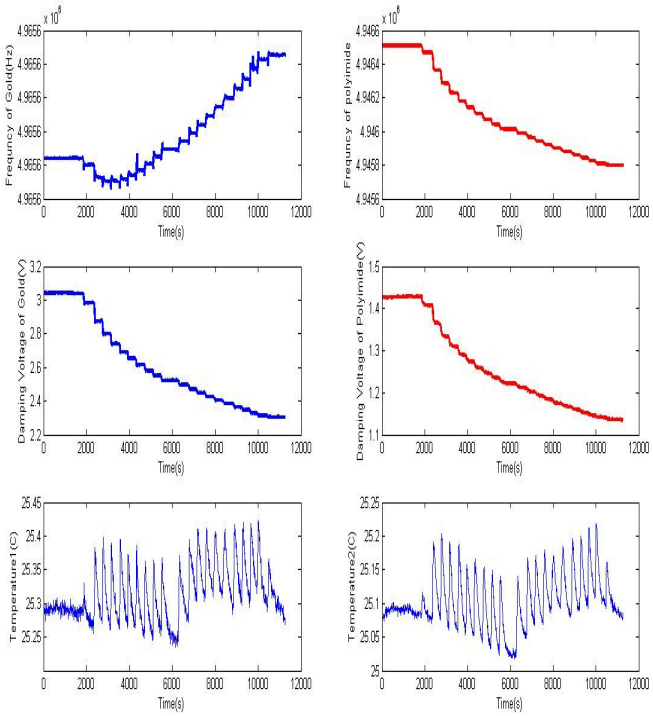

Figure 2.9.Lab View© program recording the raw data for CO_2 gas adsorption in polyimide

This plot illustrates CO_2 gas adsorption in polyimide at 25 ºC. The two top blue plots on the left are the reference QCM's frequency and damping. Conversely, the two top red plots on the right are the coated QCM's frequency and damping. The bottom two plots are the temperatures of the two thermocouples that were positioned inside the

pressure vessel. As shown in the plot, the frequency of coated the QCM decreases as the pressure inside the cell increases, as a consequence of gas adsorbed into the coated materials. On the other hand, the frequency of the reference increases as pressure inside the cell increases. The damping voltages of both crystals were used to ensure crystals were intact and functioning. As shown in the two bottom plots, the temperature gradient inside the cell at two different locations is relatively small ~ 0.2 ºC.

2.3 Experimental procedures

Both coated and uncoated QCMs were mounted on the crystal holder and placed inside the high pressure cell. The BNC cables were connect to the phase locks, and they were connected to the frequency counters and multi-meters. The setup was placed under vacuum for 20 minutes; once the frequency stabilized, the average frequency was recorded and used to measure the amount of mass deposited on the surface of the coated QCM. Once this value was recorded, the high pressure cell was covered with insulating glass fiber material and heated up to 180°C while it remained under vacuum. This step was essential to removing all the water vapor and solvents that could be present in the sample material. The cell was then cooled down to an ideal temperature for running the experiment, a step that took 6-8 hours. Once the temperature was stable, the gas outlet was closed and the vacuum was turned off. The frequencies were then monitored for both QCMs until they became stable. At this point, the frequency oscillation was less than 1 Hz. Once the frequencies were stable, one of the three gases was slowly introduced into the system until it reached a new pressure point. The frequencies were recorded in Lab

View© software and observed until they reached a steady-state value before pressure increment. This step was repeated for all the pressure steps.

CHAPTER 3

SYSTEM CALIBRATION:

3.1 Calibration of the apparatus using CO_2 gas adsorption in polyimide

To ensure the accuracy of the experimental protocol, the QCM setup was calibrated using Matrimid 5218, for which the sorption and thermodynamic properties are known.[11-13]

An amount of 0.326 g of Matrimid 5218 (USA, Hutsman) was added to 3 ml of 1-methyl-2-pyrrolidione (anhydrous 99.5%, Sigma-Aldrich) and was allowed solute to dissolve for 2 to 3 hours. Once solute was completely dissolved solution became fairly viscous and yellowish. Figure 3.1 shows the chemical structure of commercially available Matrimid 5218.

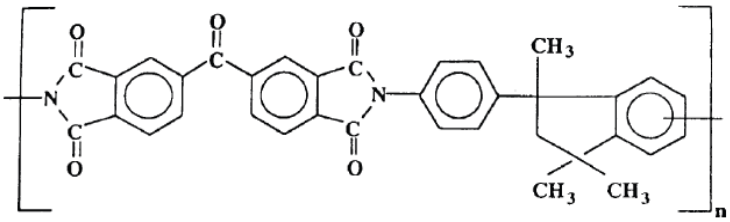

Figure 3.1. Chemical structure of Matrimid 5218

The polymer solution was then spin-coated on the QCM at 2000 rpm for 10 seconds. Next, the coated QCM was placed in the convectional vacuum oven and heated over night at 150º C under vacuum. In the end, the crystal was removed from the oven and was allowed to cool down to room temperature. To measure the mass of Matrimid deposited

on the surface of the QCM, it was placed inside the cell, under vacuum (0.75 Psi) for 30 minutes. Once the system was allowed to stabilize, the resonant frequency of the coated QCM was measured for pressure between 0 and 4 bar. Using the Sauerbrey equation (1.1) the total mass deposited on the QCM surface was calculated to be 2.9102×10^{5} ng.cm^{-2}. In order to study the uniformity and continuity of the Matrimid coating on the QCM, a Scanning Electron Microscope (SEM) was used. As shown in Figure 3.2, there are separate islands of Matrimid polymer on the surface of the crystal rather than a continuous thin film. This film discontinuity could cause some variation in the total amount of gas adsorbed in the Matrimid, since the total amount of gas adsorbed onto the surface of a solid is proportional to the total surface area of the solid and not the volume of the solid.

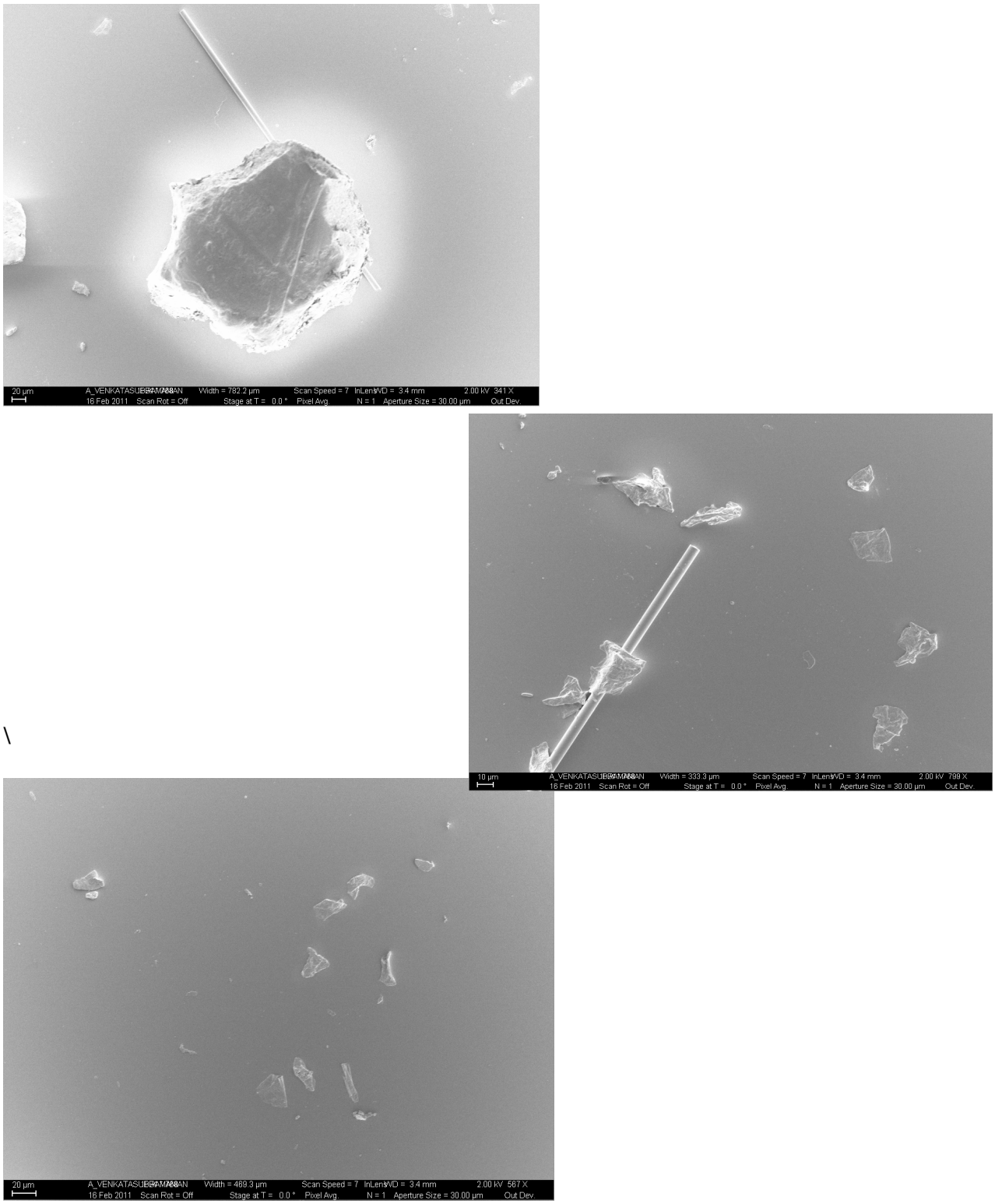

\

Figure 3.2. SEM Images of Matrimid film coated on QCM

After sample characterization, the coated and reference crystals were placed inside a high pressure cell to be degassed overnight. This step is crucial to evacuate all the gases and solvents present in the polymer. The experiment starts by letting a specific gas flow inside the high pressure cell to reach a new equilibrium condition at a specific pressure. The experiments were performed at temperatures of 25, 30, 42, and 53 ºC and pressures between 0 and 4 bar with the step pressure change of 0.2 bar for single component CO_2 gas. Monitoring the experiment with Lab View© software, the coated crystal's frequency decreases with mass loading due to adsorption of the ambient gas and increasing hydrostatic pressure inside the cell. After each experiment for different temperatures, the corrections were applied to the frequency of the coated QCM. Applying the correction, the resonant frequency change comes directly from the ambient gas absorbed into the Matrimid. Figure 3.3 shows the adsorption equilibrium isotherms plotted in terms of [CC of gas(STP)/ gram of material] as a function of pressure. In the end, each of the temperature measurements was repeated to provide repeatability of the data. As a check for consistency of the experimental data, after several months, a second data set was collected for CO_2 at 30 ºC. The two data set agree satisfactorily, but the dual model adsorption parameters differ a bit. This could be due to the age decay of the polymer.

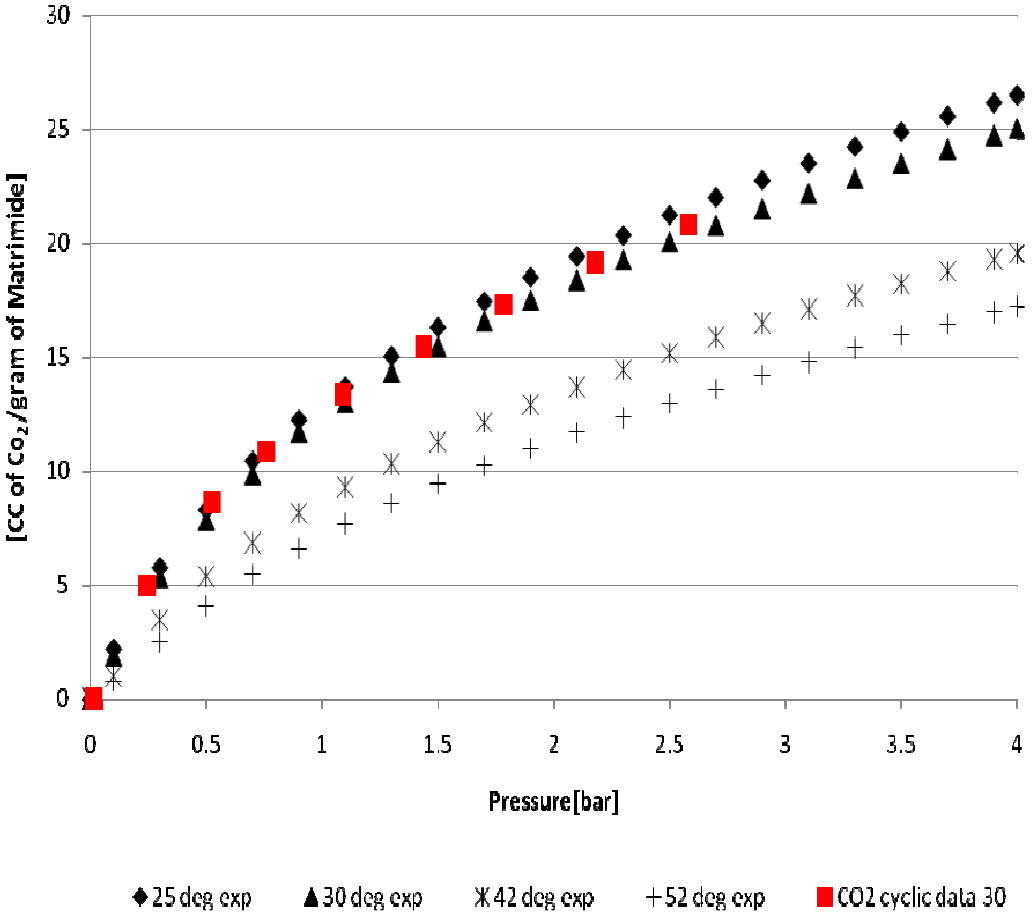

Figure 3.3. CO_2 sorption isotherm within Matrimid at different temperatures.

3.2 Dual model Langmuir adsorption model for Matrimid

The shapes of the isotherms in Figure 3.3 are characteristic of dual-mode sorption. At low pressure, the coverage varies linearly with pressure. However, coverage saturates with increasing pressure. This phenomenon is due to the density of molecules on the surface, where at low pressure the density of molecules on the surface varies linearly with coverage. However, at high coverage, the density of molecules on the surface saturates, since each molecule blocks a finite region on the surface[14]. In order to extract the sorption parameters for Matrimid, the experimental data was fit into a simple dual-model Langmuir model expressed in equation 3.1 [15].

$$C = K_D \times P + \frac{C_H \times \alpha P}{1 + \alpha P} \tag{3.1}$$

Where C [cm^3 (STP)/ cm^3 (polymer)] is the equilibrium concentration, K_D [cm^3 (STP)/ cm^3(polymer)Psi] is the Henry's-law solubility constant, C_H [cm^3 (STP)/ cm^3(polymer)] is the maximum Langmuir capacity constant, α is the Langmuir affinity constant (Psi^{-1}), and P is the Pressure(Psi). Figure 3.4 and Table 3.1. present a fit of the experimental data to the dual-mode Langmuir model (3.1) with nonlinear regression technique, the dual-mode Langmuir model curves and parameters.

Table 3.1. Dual-Mode parameters of CO_2 sorption in polyimide film

Temperature©	***α*** *(1/Psi)*	***K_D*** *[*cm^3 (STP)/ cm^3(polymer)]	***C_H****[*cm^3 (STP)/ cm^3(polymer)]
25	1.00	2.38	21.24
30	0.95	2.09	21.04
42	0.73	1.89	16.12
52	0.54	1.66	15.46

The results tabulated in Table 3.1 illustrate that by increasing the temperature ($T<T_g$) for a fixed gas affinity constant, the adsorption capacitance and the Henry constant both decrease.

Furthermore, the experimental data was fitted into the global dual-mode Langmuir model represented in equation 3.2, and the thermodynamic properties of the polyimide are reported in Table 3.2

$$c = (\beta_0 T + \beta_1).P + \frac{C_H \times \alpha_0 \times \exp\left(\frac{-\Delta H_a}{RT}\right)P}{1 + \alpha_0 \times \exp\left(\frac{-\Delta H_a}{RT}\right)P}$$
$$K_D = (\beta_0 T + \beta_1) \qquad (3.2)$$

where K_D is Henry's-law solubility constant which assumed to vary linearly with temperature.

Table 3.2 Thermodynamic parameters of CO_2 sorption for polyimide film

β_1	15.38
β_0	-0.044
C_H[cc/ cc]	21.8
α_0	2.3E-06
ΔH(kJ.mol^{-1})	-32.01

substituting the parameters β_1 and β_0 back to equation 3.2, the Henrys constant for polyimide is calculated and summarized in Table 3.3

Table 3.3 Henry's constant of CO_2 sorption in polyimide film

Temperature °C	**K_D[cc/ cc.psi]**
25	2.405348
30	2.187806
42	1.665705
52	1.230621

The Dual-Mode parameters of CO_2 sorption in polyimide film were used to fit into the experimental data, and the results are plotted in figure 3.4.

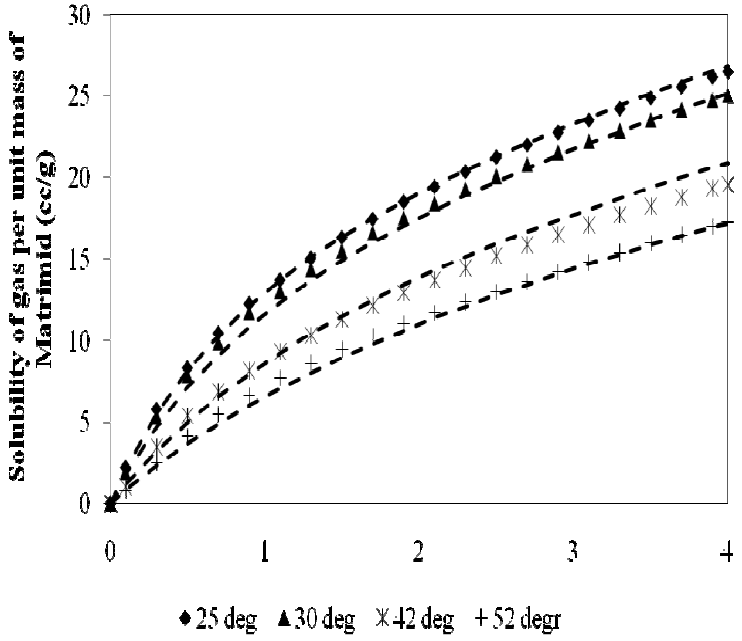

Figure 3.4. Experimental data fitted into global dual mode Langmuir

As shown in the plot, the experimental data fitted the global dual model Langmuir model adequately.

3.3 Experimental data comparison with literature data

Furthermore, the experimental data at different temperatures are compared to the available data from Moore[12] and Chung[11]. The data clearly shows good agreement with the data reported in the literature. However, there is a slight difference between the curves. This might be due to the differences in Polyimide membrane, physical aging, or uniformity of the membrane.

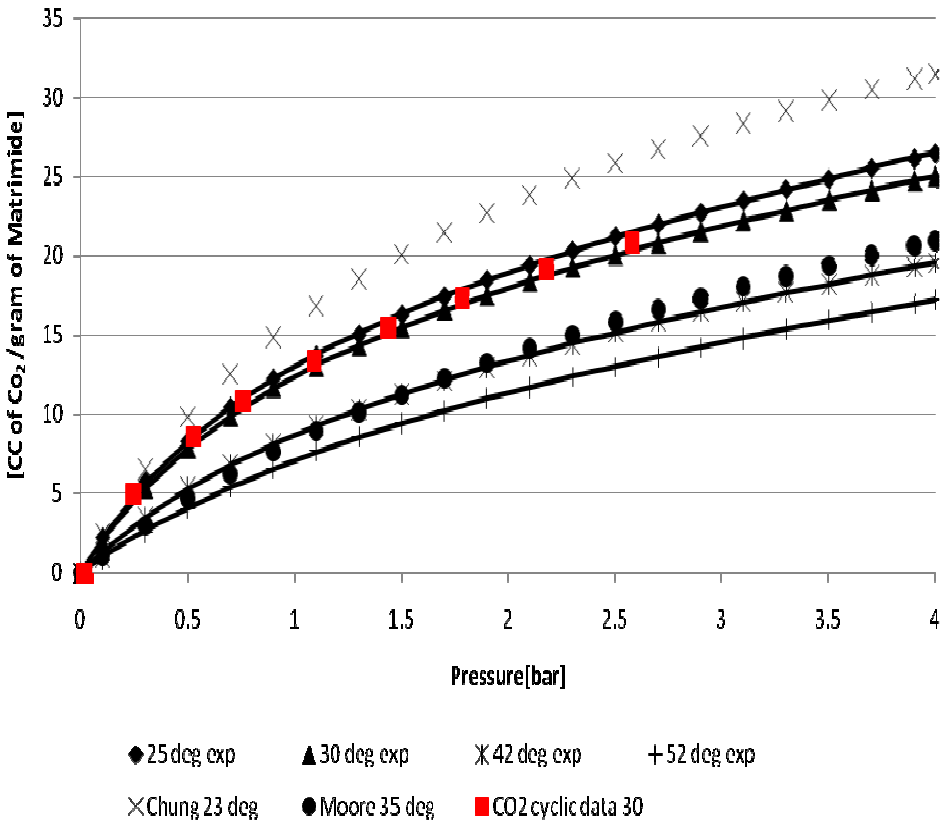

Figure 3.5. Comparison between the experimental CO_2 sorption isotherms and literature data isotherms within Matrimid

CHAPTER 4

GAS ADSORPTION IN ALUMINOSILICATE NANOTUBES

4.1 Sample deposition

Aluminosilicate nanotube solution was cast onto the surface of QCM. 100 µL of the solution was pipetted on the surface of the QCM, and it was baked in a conventional oven at 75 ºC over night. Following the deposition, the QCM sample was prebaked in the conventional oven at 185 ºC for 1 hour; hence, most the solvents trapped inside the nanotubes were evaporated. Both the sample QCM and the reference QCM were placed inside the high pressure cell and then heated to 185 ºC under vacuum to ensure all the solvents and moisture were evaporated. The high pressure cell was placed under vacuum and was heated for 12 hours before it cooled down to room temperature. The mass of aluminosilicate nanotubes deposited on the QCM was calculated using the Sauerbrey equation (1.2)

4.2 Sample characterization

4.2.1 SEM characterization

The uniformity and continuity of the aluminosilicate film deposited on the surface of the QCM was characterized using SEM. SEM images in Figure 4.1 show the surface of a QCM after film deposition, and it is listed in table 4.1.

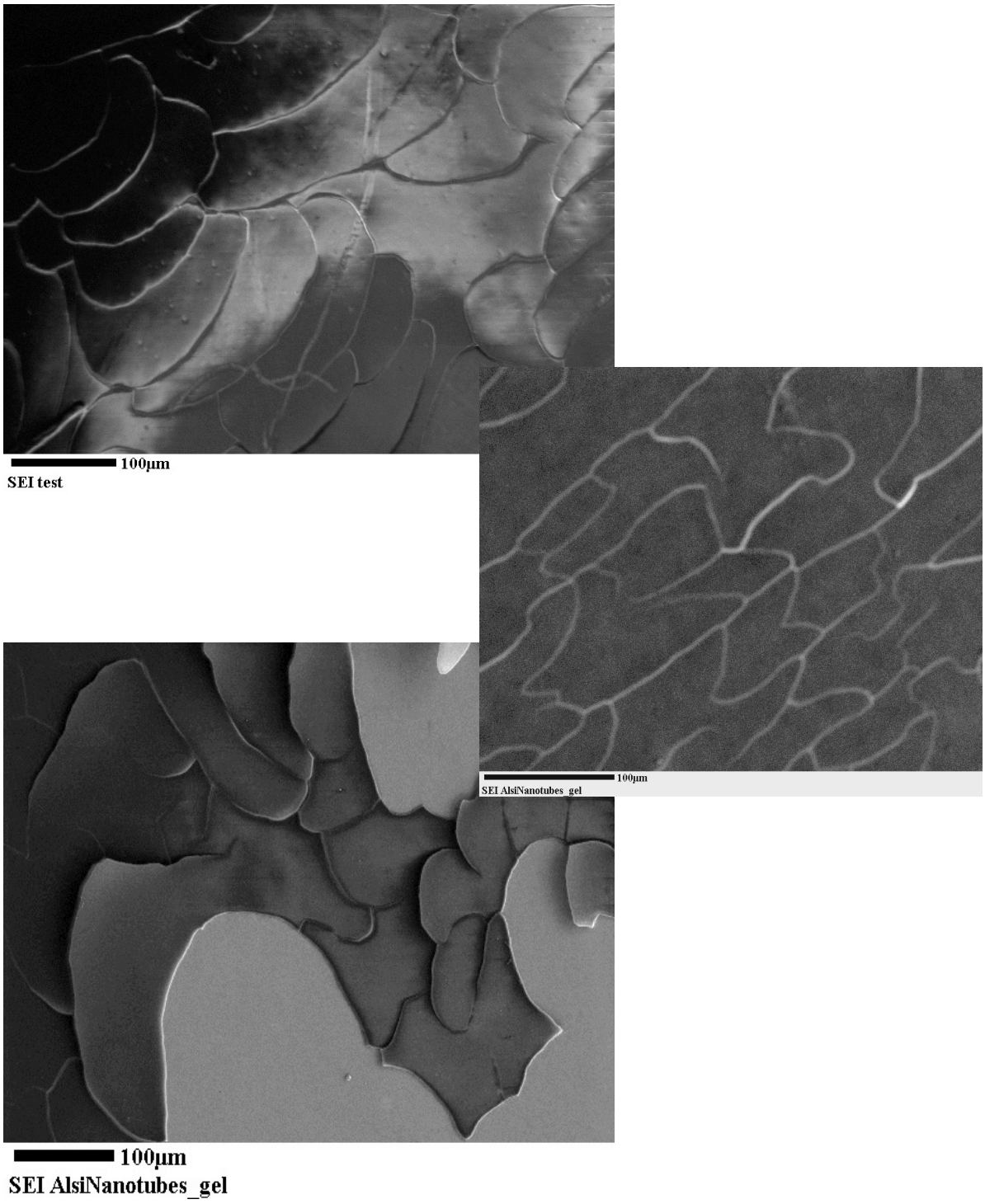

Figure 4.1. SEM Images of Sample NT012

The SEM images in Figure 4.1 show that the film is continuous; however, it is not uniform. In the center of the QCM, the film thickness is fairly higher compared to the edges. The plates shown in the SEM images are rows of aluminosilicate nanotubes aligned on top of each other. The thickness of these plates varies between 0.5 µm and 1 µm.

4.2.2 XRD characterization:

To study the effects of gas adsorption on the thin film of aluminosilicate nanotubes, X- Ray Diffraction(XRD) of the sample, before and after each experiment, was obtained.

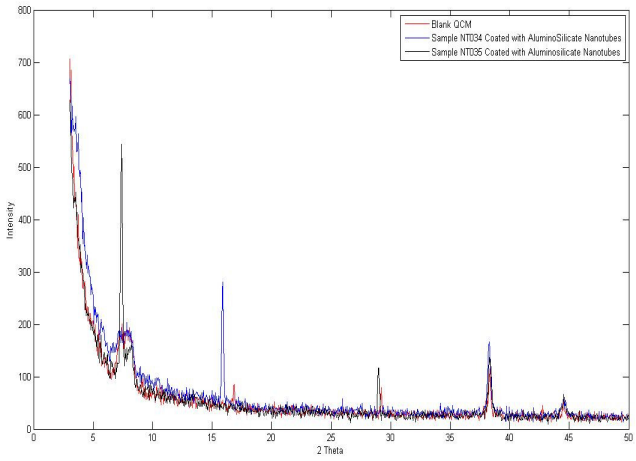

Figure 4.2. XRD characterization of Sample NT034

Figure 4.2.shows the XRD Pattern of an uncoated QCM and aluminosilicate coated QCMs (samples NT034 and NT035). The peaks for gold substrate were visible for all three QCMs at 38 and 44 angles; however, the peaks for aluminosilicate nanotubes weren't apparent. This could be due to the homogeneity of the film and mainly insufficient amount of aluminosilicate nanotubes deposited on the both samples.

4.3 Adsorption measurement

Gas adsorption measurements were conducted on different aluminosilicate nanotubes samples. All the samples were prepared as described in section 4.1. The total mass of aluminosilicate nanotubes deposited on the QCMs used in this study is calculated using the Sauerbrey equation and summarized in Table 4.1.

Table 4.1. Samples used for gas adsorption isotherm measurement

Sample Number	**mass(μg/cm^2)**	**Gas measurement**	
Sample NT005	147	CO_2, N_2	
Sample NT017	94.0	CO_2, N_2	
Sample NT032	91.0	CO_2, N_2,CH_4	
Sample NT034	20.6	CO_2, N_2,CH_4	gas cycle at 30ºC
Sample NT041	16.6	CO_2, N_2,CH_4	gas cycle at 45ºC
Sample NT042	83.1	CO_2, N_2,CH_4	gas cycle at 69ºC

The first three samples were used for the entire gas adsorption experiment; it consists of testing the samples for different gases at different temperatures. The disadvantage of using one sample is that it could be decomposed over the time period that the experiment was conducted. Therefore, the last three samples were each investigated at a specific temperature for three different gases. At the end of each cycle the initial test was repeated to confirm the sample functionality. The CO_2 gas experiment was performed at temperatures of 22, 42, 58, and 68 ºC and at pressures between 0 and 8 bar with the step pressure change of 0.2 bar for sample NT005. Figure 4.3 shows the adsorption equilibrium isotherms plotted in terms of [CC of gas(STP)/ gram of material] as a function of pressure.

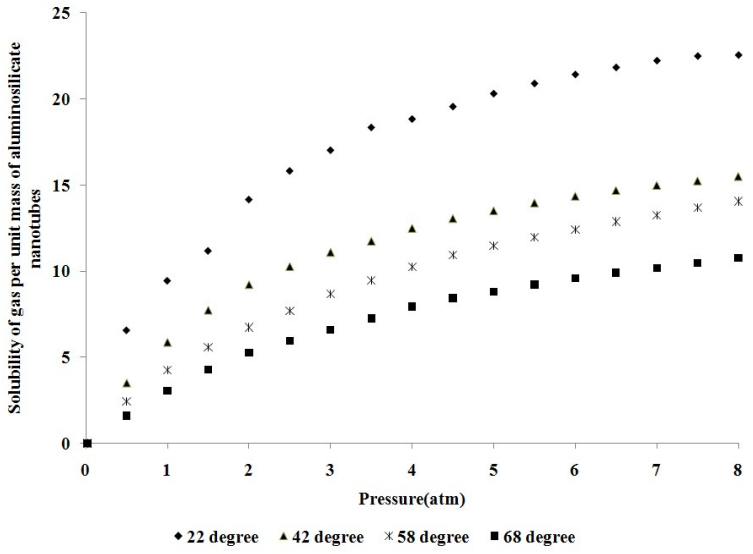

Figure 4.3. CO_2 gas adsorption in aluminosilicate nanotubes sample NT005

Figure 4.3 shows the CO_2 gas adsorption in aluminosilicate nanotubes (Sample NT005) at four different temperatures. In order to confirm the repeatability of the experimental data, CO_2 gas adsorption of four samples was conducted at 30 ºC and is illustrated in Figure 4.4.

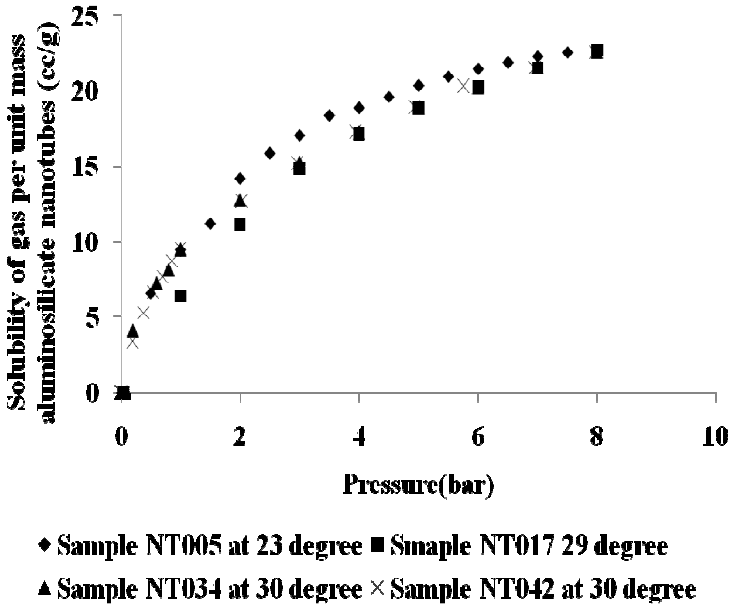

Figure 4.4. Gas adsorption of different samples at the same temperature.

As shown in the figure, there is a reasonable consistency between the amount of gas adsorbed per mass of nanotubes for all samples; hence, the CO_2 gas isotherms for different samples were used to fit into the models. Figure 4.5 shows the CO_2 gas isotherms in aluminosilicate nanotubes for Samples NT005, NT034, NT041, NT017, and NT042. The same experiment was repeated for CH_4 and N_2 gas. The results are shown in Figure 4.6 and Figure 4.7 respectively.

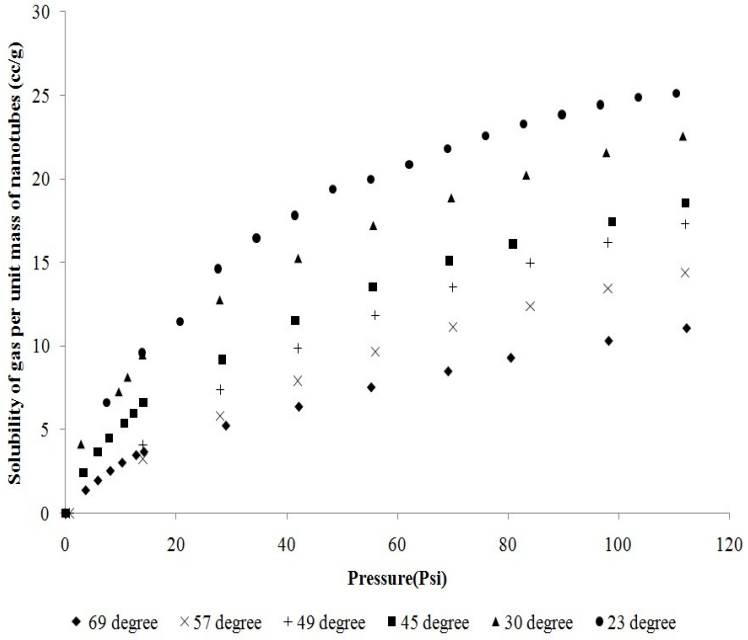

Figure 4.5. CO_2 gas adsorption in aluminosilicate nanotubes

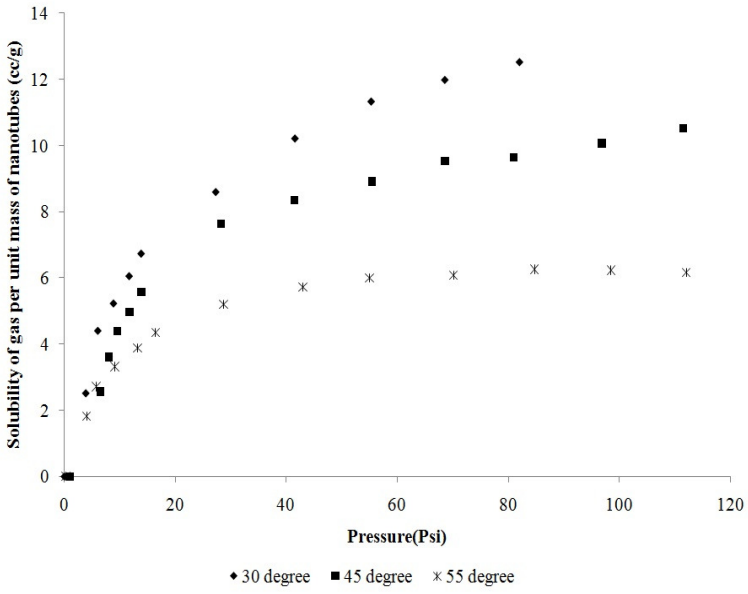

Figure 4.6. CH_4 gas isotherms for aluminosilicate nanotubes Samples NT034, NT041 and NT042

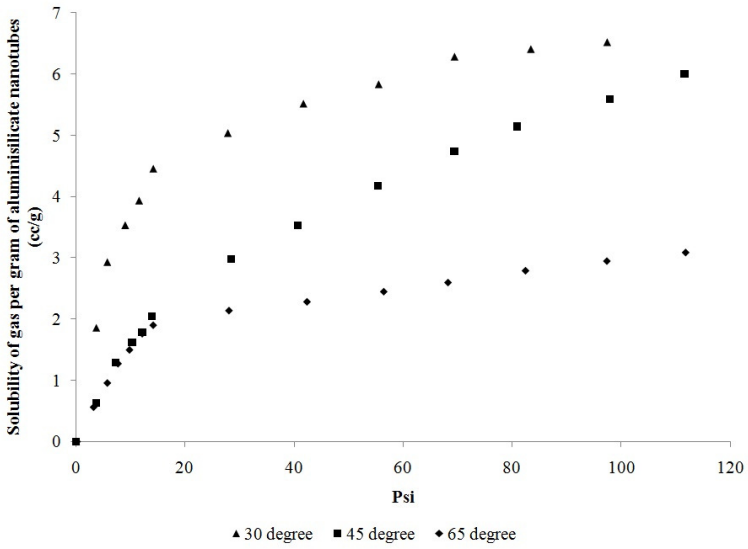

Figure 4.7. N_2 gas isotherms for aluminosilicate nanotubes NT034, NT041 and NT042

To confirm the sample robustness over the period of the gas experiment, a complete gas cycle test was done for each sample as described earlier. For instance, sample NT034 was tested for CO_2, and N_2 at a fixed temperature of 30º C. After completion of the gas cycle, the sample was tested for CO_2 again to validate that the data are repeatable and also that the sample is still in good condition. The results are presented in Figure 4.8.

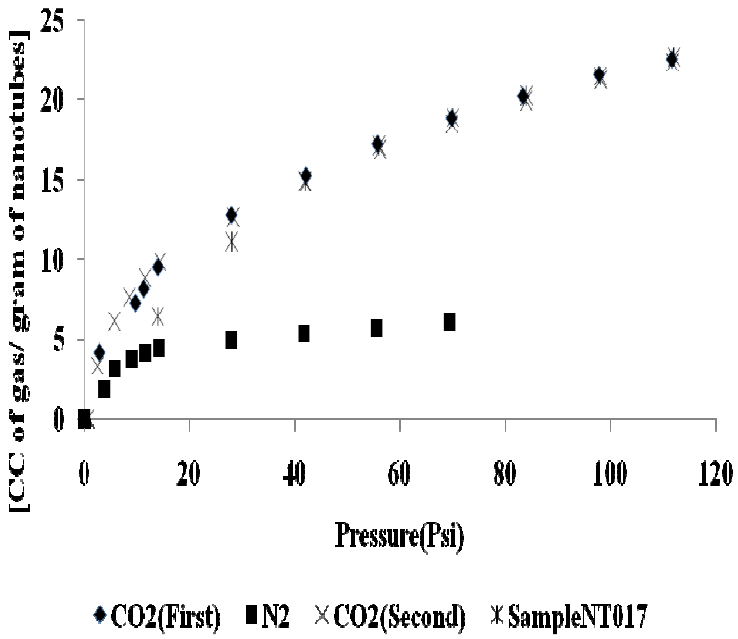

Figure 4.8. Gas cycling for Sample NT034 at 30ºC

4.4 Simple Langmuir adsorption model for aluminosilicate nanotubes

The shapes of the isotherms in Figure 4.3 are characteristic of simple Langmuir adsorption. In order to derive an expression for the amount of gas adsorbed on to the coated film on the surface of QCM as a function of partial pressure, some assumptions were made. These assumptions are:

1) the adsorbing gas adsorbs into an immobile state,
2) all sites are equivalent,
3) each site can hold at most one molecule, and
4) there is no interaction between adsorbent molecules on adjacent sites so that α will be independent of the coverage of the adsorbed species[14].

Using the above assumptions, equation 4.1 is obtained as shown below.

$$C = \frac{C_H \times \alpha P}{1 + \alpha P} \tag{4.1}$$

where C [cm^3 (STP)/ cm^3 (polymer)] is the equilibrium concentration, C_H [cm^3 (STP)/ cm^3(polymer)]is the maximum Langmuir capacity Constant, α is the Langmuir affinity constant (Psi^{-1}), and P is the Pressure(Psi). Equation 4.1 is the simple Langmuir adsorption isotherm for noncompetitive adsorption. This equation predicts that at low pressure the coverage varies linearly with pressure; this linearity at low pressure is explained by Henrys Law as shown in Equation 4.2.

$$C = K_H P \tag{4.2}$$

where C is the solubility of gas per unit mass of aluminosilicate nanotubes (cc/g), P is the pressure in psi, and K_H is Henry's constant (cc/g.psi). This equation was used to fit the gas adsorption isotherms of the experimental data at low pressure.

In order to extract the heat of adsorption, the affinity constant was assumed to vary with temperature according to equation 4.3.

$$\alpha = \alpha_0 \times e^{(\frac{-\Delta H_a}{RT})} \tag{4.3}$$

where ΔH_a is the Heat of Adsorption (kJmol^{-1}), α_0 is the temperature independent Langmuir affinity constant, R is universal gas constant (8.314 kJmol^{-1}K^{-1}) ,and T is the gas temperature(K).In order to extract the gas sorption parameters of aluminosilicate nanotubes, the experimental data was fitted into the simple Langmuir model, and the heat of adsorption equation was extracted.

4.4.1 CO_2 gas adsorption in aluminosilicate nanotubes

Sorption isotherms for CO_2 gas at six different temperatures were used to extract the sorption parameters for aluminosilicate nanotubes using two techniques:

a) Individual fit, and

b) Global fit,

In the individual fit, the experimental data was fitted to equation 4.1 for each individual curve for a constant temperature, and the values of C_H, and α were determined using a nonlinear regression technique. Then, the average of C_H values of the curves was calculated. This average was used to fix the C_H value for each individual curve. The nonlinear regression technique was used to determine the value of α for each curve at a

fixed C_H value. Table 4.2 presents the affinity constant of each curve, for fixed capacity constant of 26.4 CC/CC as a function of temperature.

Table 4.2. Affinity constant of aluminosilicate nanotubes for CO_2 gas

Temperature(°C)	α(1/Psi)
69	0.007
57	0.010
49	0.015
45	0.020
30	0.038
23	0.046

Once Log(α) is plotted against 1/T, a linear relation is observed, which in fact indicates constant heat of adsorption, as shown in Figure 4.9.

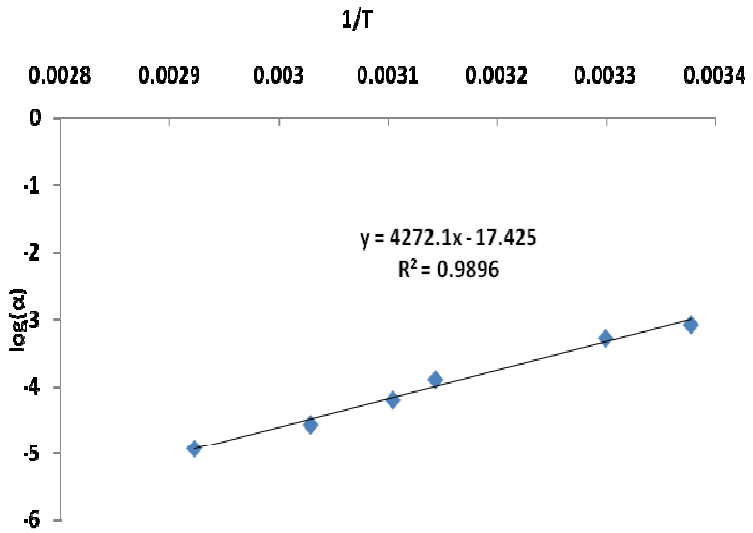

Figure 4.9. Linear fit of CO_2 gas data into Equation 4.2

Using the slope of the linear fit, thermodynamic parameters of aluminosilicate nanotubes for CO_2 gas were calculated and reported in Table 4.2.

Table 4.3. Thermodynamic properties of aluminosilicate nanotubes for CO_2

Thermodynamic parameters	**Individual Fit**
C_H (cc/cc)	26.6
α_0 (1/psi)	1.54E-08
ΔH_a (kJmol^{-1})	-36.7

Since the maximum Langmuir capacity is fixed in individual fits, for higher and lower temperatures these fits do not produce good results. Therefore, a global fit was used by combining equation 4.1 and equation 4.2 Equation 4.3; equation 4.4 shows the global fit expression. In this fit three variable, C_H, α_0, and ΔH_a *are* optimized independently.

$$c = \frac{C_H \times \alpha_0 \times \exp\left(\frac{-\Delta H_a}{RT}\right) P}{1 + \alpha_0 \times \exp\left(\frac{-\Delta H_a}{RT}\right) P} \tag{4.4}$$

The Langmuir parameters were obtained from numerical optimization, as well as minimizing the sum of squares of deviations between the experimental concentration and calculated concentration points for six CO_2 gas isotherms at different temperatures. The initial guess values for the variable parameters were obtained from the linear fit method value reported in the previous section. Table 4.4 summarizes the thermodynamic parameters of aluminosilicate nanotubes for CO_2 gas using the global fit method.

Table 4.4. Thermodynamic properties of aluminosilicate nanotubes for CO_2 gas using the global fit method

Thermodynamic parameters	**Global Fit**
C_H (cc/cc)	32.0
α_0 (1/psi)	5.03E-08
ΔH_a (kJmol^{-1})	-32.9

Using the parameters reported in Table 4.4, the Langmuir model isotherms were generated and used to calculate the error. The standard deviation between the experimental sorption and the Langmuir model sorption was calculated for each data set according to Equation 4.5.

$$\sigma = \sqrt{\frac{1}{N-1}\sum_{j=1}^{N}(C_{\exp} - C_{Langmuir})^2} \tag{4.5}$$

where N is the number of data, $C_{\exp}$ is the experimental sorption, and $C_{Langmuir}$ is the Langmuir model sorption. The standard deviation for each temperature for CO_2 gas calculated in Table 4.5.

Table 4.5. Standard deviation of experimental data using global fit model

Temperature °C	σ cm^3(STP)/cm^3
23	0.57
30	1.38
45	1.02
49	0.47
57	0.66
69	0.95

Figure 4.10 presents the experimental adsorption isotherms of CO_2 gas in aluminosilicate nanotubes at six different temperatures. The fitted CO_2 gas isotherms with global fit model are the dashed lines in Figure 4.10.

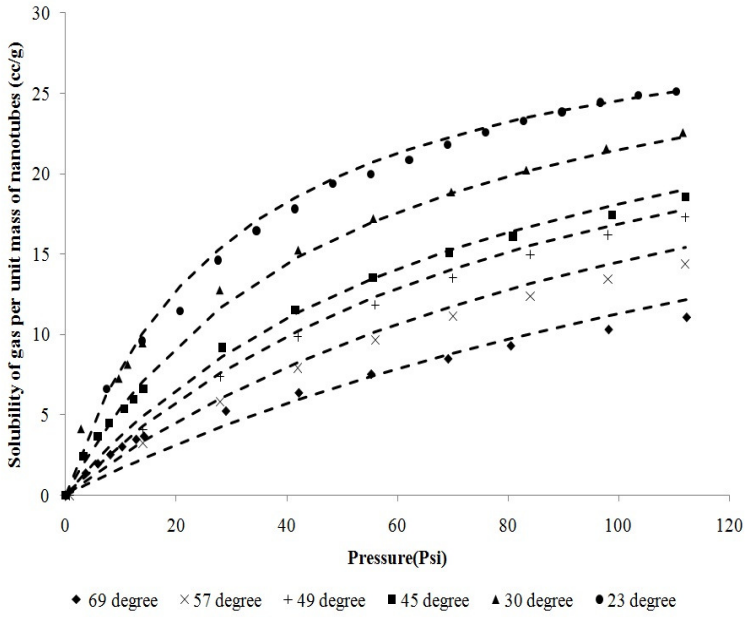

Figure 4.10. CO_2 gas adsorption in aluminosilicate nanotubes.

4.4.2 CH_4 gas adsorption in aluminosilicate nanotubes

The same methods were applied to the experimental data obtained from pure CH_4 gas adsorption at three different temperatures. Each individual curve was fitted into equation 4.1, and the results are presented in Table 4.6. The sigma between the experimental data and the Langmuir model was calculated for each sorption data set according to Equation 4.5.

Table 4.6. Sorption parameters of aluminosilicate nanotubes for CH_4 gas

Temperature(C)	***α (1/Psi)***	C_H[cm^3 (STP)/ cm^3]	***σ***
30	0.059	14.8	0.26
45	0.056	12.0	0.3
55	0.10	6.92	0.16

Small errors in measuring the concentration of the adsorbed gas into the film were attributed to the pressure transducer and pressure reader employed in the experimental setup. As shown in the above table, the maximum Langmuir capacity constant decreases with increasing the temperature as expected. Figure 4.11 illustrates the CH_4 gas adsorption isotherms at three different temperatures. The dashed lines in the Figure are the individual fit model.

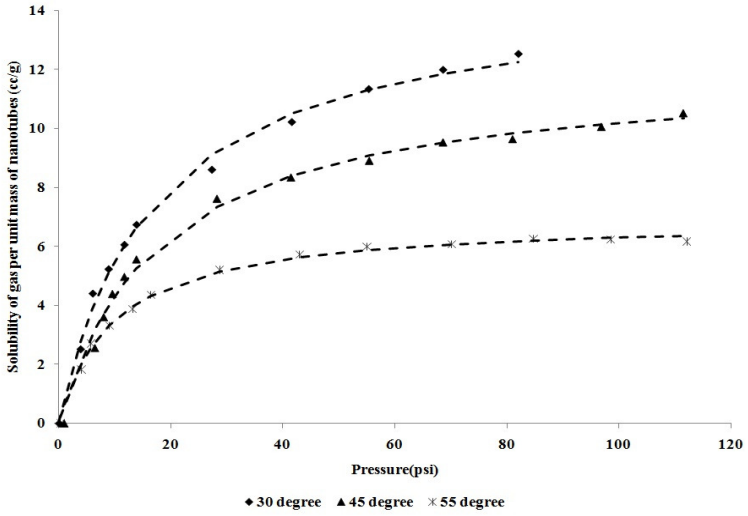

Figure 4.11. CH_4 gas adsorption in aluminosilicate nanotubes for Sample NT034, NT041, and NT042.

The experimental data obtained for CH_4 was fit into the global model; however, the global fit model did not converge. This problem occurs because the Langmuir model used to fit the experimental data does not work for CH_4 gas adsorption in aluminosilicate nanotubes. A better model needs to be developed.

4.4.3 N_2 gas adsorption in aluminosilicate nanotubes

The experimental data was obtained for N_2 gas adsorption in samples NT034, NT041, and NT042. The experimental data was fit into Langmuir model using individual fit as shown in Figure 3.13.

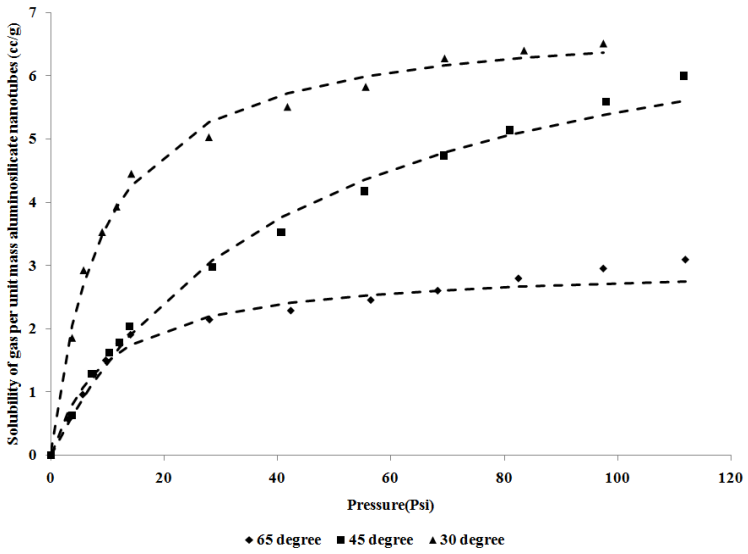

Figure 4.12. N_2 gas adsorption in aluminosilicate nanotubes for Sample NT034, NT041, and NT042 with individual Langmuir fit

The N_2 gas adsorption at low pressure and high temperature is dominated by noise; hence, the data collected for N_2 at 65 and 45º C are not satisfying. N_2 gas solubility in aluminosilicate nanotubes is very low compared to CH_4 and CO_2. However, to compare the thermodynamic properties of these gases, the experimental data for N_2 was fit into the global model using equation 4.4. The results are plotted and summarized in Figure 4.14 and Table 4.8.

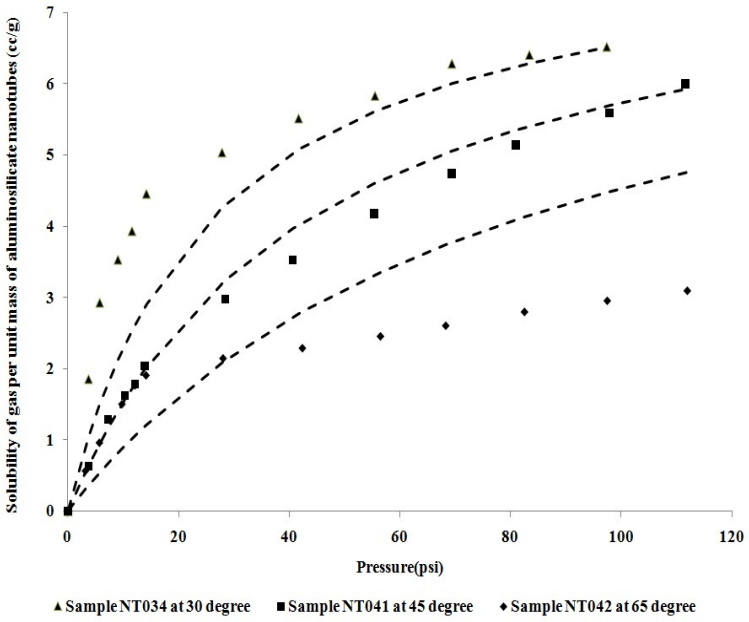

Figure 4.13. N_2 gas adsorption in aluminosilicate nanotubes for Sample NT034, NT041, and NT042 with global Langmuir fit

Table 4.7. Thermodynamic properties of aluminosilicate nanotubes for N_2 gas

Thermodynamic parameters	**Global Fit**
C_H (cc/cc)	8.26
α_0 (1/psi)	5.65E-07
ΔH_a (kJmol^{-1})	-28.1

4.5 Henry's fit

In order to compare the selectivity of a specific gas in aluminosilicate nanotubes, the gas adsorption isotherms were fit into Henry's fit model at pressure range between 0.1 and 13 psi. As discussed earlier, gas adsorption isotherms are linear at low pressure; therefore, Henry's law could be used to extract the Henry's constant at different temperatures for different gases. Table 4.8 summarizes these findings.

Table 4.8. Henry's constant at low pressure.

K_H (cc/g.psi)	**30°**	**45°**
CO_2	1.86	0.84
CH_4	0.93	0.46
N_2	0.72	0.20

There is a higher selectivity for CO_2 gas over two other gases at 30 and 40º C. However, at higher temperature there is no major selectivity between these gases. The selectivity of CO_2 to CH_4 is calculated to be 2.0, and selectivity with respect to nitrogen is 2.6 at room temperature (30ºC) and decreases at higher temperatures.

CHAPTER 5

CONCLUDING REMARKS

5.1 Conclusions

In this research, a QCM based high pressure setup was designed for gas adsorption and diffusion on thin films of micro porous materials and nanotubes. The setup presented here is highly sensitive and accurate to the mass absorbed on the surface of the QCM and simultaneously accessible and compact. The total cost of the setup was estimated to be less than $50,000 which makes it economical.

The high pressure apparatus was calibrated using Matrimid 5218. Adsorption of CO_2 in Matrimid thin film was conducted at temperatures between 25 and 52 ºC and pressure ranging between 0 and 4 bar. The CO_2 adsorption isotherms were fit into the dual-mode adsorption model and the parameters for Matrimid were reported. The dual-mode model fits the experimental data satisfactorily. Comparing the experimental adsorption isotherm of Matrimid for CO_2 gas with literature data shows reasonable agreement between the experimental and literature data. This comparison shows the ability of the QCM based setup to produce data with high level of accuracy in thin films.

In this work, the adsorption parameters of aluminosilicate nanotubes were observed. The adsorption of CO_2, N_2, and CH_4 gases on aluminosilicate nanotubes samples has been studied in the temperature range of 20° to 120°C and the pressure range of 0 to 8 bar. The gas adsorption isotherms obtained for aluminosilicate nanotubes were fit into the Langmuir model; in addition, adsorption parameters and thermodynamic

properties of this material were reported. The Langmuir adsorption model for CO_2 and N_2 fits the aluminosilicate nanotubes sorption data adequately; hence, the parameters extracted from this model could be used to estimate the thermodynamic parameters associated with the adsorption. The experimental results yield CO_2 and N_2 heats of adsorption of -32.9 and -28.1 kJ/mol respectively. However, the Langmuir sorption model for CH_4 gas did not fit the aluminosilicate nanotubes sorption. Future work is required to develop a model that fits the CH_4 gas adsorption isotherms.

In the end, the gas adsorption isotherms were fitted by an effective Henry's law constant. From this constant, a preferentially high selectivity for CO_2 gas adsorption over the other two gases was observed.

5.2 Recommended future work

In this section some recommended future work and possible extensions are discussed.

a) The current setup sensitivity could be enhanced by employing a QCM with higher resonant frequency and Q factor to improve the frequency change to noise ratio. However crystals would have to be made in house for this with thinner quartz, the commercial crystals are available in 5 and 9 MHz. Using higher frequency QCM may also lower the limit of gas concentration detection to be suitable for inert gas adsorption studies.

b) The current setup does not have a fixed crystal holder. The crystal holder designed in this setup is set into an arbitrary position within the chamber. Placing the crystals in the same position may improve the repeatability of the data.

c) The simple Langmuir model used in this work needs to be extended in order to fit different gas adsorption isotherms. This model fits the CO_2 and N_2 gas isotherms adequately; however, a more complicated model is required to fit the CH_4 gas isotherms.

d) The aluminosilicate nanotubes studied in this work could be functionalized to have a better selectivity for different gases. More studies of these nanotubes are required in order to clarify the effect of these functionalizations.

APPENDIX A: GLOBAL FITTING CODE

```
clear all
clc
pressure=zeros(6,9);
pressure(1,:)=[0.0800   13.8000   27.6000   41.4000   55.2000   69.0000
82.8000   96.6000  110.4000];
pressure(2,:)=[0.0400   13.9600   27.9100   42.0800   55.6500   69.7500
83.3000   97.7500  111.6000];
pressure(3,:)=[0.0100   14.1000   28.3100   41.5000   55.5300   69.3600
80.8400   98.7300  112.0000];
pressure(4,:)=[0.7500   14.0000   28.0000   42.0000   56.0000   70.0000
84.0000   98.0000  112.0000];
pressure(5,:)=[0.7500   14.0000   28.0000   42.0000   56.0000   70.0000
84.0000   98.0000  112.0000];
pressure(6,:)=[0.0500   14.1800   28.9800   42.1500   55.2200   69.1200
80.4500   98.1200  112.2000];



data=zeros(6,9);
data(1,:)=[ 0    9.6074   14.6231   17.8198   19.9739   21.7985
23.2725   24.4373   25.1236];
data(2,:)=[ 0    9.4648   12.7439   15.2363   17.1957   18.8491
20.2106   21.5560   22.5430];
data(3,:)=[ 0    6.6139    9.1791   11.5307   13.5479   15.0911
16.1029   17.4330   18.5424];
data(4,:)=[ 0    4.0820    7.3762    9.8652   11.8405   13.5078
14.9627   16.1981   17.2956];
data(5,:)=[ 0    3.2517    5.8306    7.9260    9.6621   11.1241
12.3721   13.4500   14.3902];
data(6,:)=[ 0    3.6856    5.2425    6.3758    7.5329    8.4851
9.2935   10.3012   11.0589];




R=8.315;
CH=30:0.01:35;
%CH=25;
alpha0=(1:0.1:10)*10^(-8);
%alpha0=10^(-5);
del_H_a=-(32:0.01:35)*10^3;
%del_H_a=-32*10^3;
temp=[23 30 45 49 57 69];
temp=temp+273;
lCH=length(CH);
la=length(alpha0);
ld=length(del_H_a);
```

```
error=zeros(lCH,la,ld);


for a=1:length(CH)
     for b=1:length(alpha0)
        for c=1:length(del_H_a)

                c_h=CH(a);

                delha=del_H_a(c);
                alpha=alpha0(b)*exp(-delha./(R*temp));
                alpha_m=alpha'* ones(1,9);


error(a,b,c)=sum(sum((c_h*alpha_m.*pressure./(1+alpha_m.*pressure)-
data).^2));



        end
    end
end

x=find(error==min(min(min(error))));

x3=(floor(x/(la*lCH)))+1;
x=x-(x3-1)*(la*lCH);
x2=floor((x/lCH))+1;
x1=x-(x2-1)*lCH+1;
ch_found=CH(x1)
alpha_found=alpha0(x2)
delh_found=del_H_a(x3)
min_error=min(min(min(error)))
```

REFERENCES

1. Arnau, A., *Piezoelectric Transducers And Application*2004: Springer.
2. Steinem, C., Janshoff, Andreas. , *Piezoelectric Sensors*. Springer Ser Chem Sens Biosens. Vol. 05. 2007. 111-149.
3. Keiji Kanazawa, K. and J.G. Gordon, *The oscillation frequency of a quartz resonator in contact with liquid.* Analytica Chimica Acta, 1985. **175**: p. 99-105.
4. Yang, M. and M. Thompson, *Surface morphology and the response of the thickness-shear mode acoustic wave sensor in liquids.* Langmuir, 1993. **9**(8): p. 1990-1994.
5. Tsionsky, V. and E. Gileadi, *Use of the Quartz Crystal Microbalance for the Study of Adsorption from the Gas Phase.* Langmuir, 1994. **10**(8): p. 2830-2835.
6. Akitt, J.W., *MULTINUCLEAR STUDIES OF ALUMINUM COMPOUNDS.* Progress in Nuclear Magnetic Resonance Spectroscopy, 1989. **21**: p. 1-149.
7. Abidin, Z., N. Matsue, and T. Henmi, *Differential formation of allophane and imogolite: experimental and molecular orbital study.* Journal of Computer-Aided Materials Design, 2007. **14**(1): p. 5-18.
8. Barron, P.F., et al., *DETECTION OF IMOGOLITE IN SOILS USING SOLID-STATE SI-29 NMR.* Nature, 1982. **299**(5884): p. 616-618.
9. Ma, L.Q. and W.B. Lin, *Designing Metal-Organic Frameworks for Catalytic Applications*, in *Functional Metal-Organic Frameworks: Gas Storage, Separation and Catalysis*2010, Springer-Verlag Berlin: Berlin. p. 175-205.
10. Kang, D.-Y., et al., *Dehydration, Dehydroxylation, and Rehydroxylation of Single-Walled Aluminosilicate Nanotubes.* ACS NANO, 2010. **4**(8): p. 4897-4907.
11. Chung, T.S., et al., *Characterization of permeability and sorption in Matrimid/C-60 mixed matrix membranes.* Journal of Membrane Science, 2003. **211**(1): p. 91-99.
12. Moore, T.T. and W.J. Koros, *Gas sorption in polymers, molecular sieves, and mixed matrix membranes.* Journal of Applied Polymer Science, 2007. **104**(6): p. 4053-4059.
13. Scholes, C.A., et al., *Sorption of Methane, Nitrogen, Carbon Dioxide, and Water in Matrimid 5218.* Journal of Applied Polymer Science, 2010. **117**(4): p. 2284-2289.
14. Masel, R.I., *Principles of adsorption and reaction on solid surfaces*1996, New York: Wiley.
15. Barrer, R.M., J.A. Barrie, and J. Slater, *Sorption and diffusion in ethyl cellulose. Part III. Comparison between ethyl cellulose and rubber.* Journal of Polymer Science, 1958. **27**(115): p. 177-197.